Available online at www.sciencedirect.com
SCIENCE DIRECT®
PERGAMON
Polyhedron 22 (2003) 2395–2400
POLYHEDRON
www.elsevier.com/locate/poly

Mn_{12} single-molecule magnets incorporated into mesoporous MCM-41 silica

M. Clemente-León [a], E. Coronado [a,*], A. Forment-Aliaga [a], J.M. Martínez-Agudo [a], P. Amorós [b]

[a] *Instituto de Ciencia Molecular, Universidad de Valencia, Doctor Moliner, 50 E-46100 Burjassot, Spain*
[b] *Instituto de Ciencia de Materiales, Universidad de Valencia, E-46071 Valencia, Spain*

Received 10 October 2002; accepted 28 December 2002

Abstract

The incorporation of four Mn_{12} derivatives, namely $[Mn_{12}O_{12}(O_2CR)_{16}(H_2O)_4]$ (R = CH_3 (**1**), CH_3CH_2 (**2**), C_6H_5 (**3**), C_6F_5 (**4**)), into the hexagonal channels of the MCM-41 mesoporous silica have been studied. Only the smallest clusters **1** and **2** that are those with compatible size with the pores of MCM-41 could be incorporated into the mesoporous silica. Powder X-ray diffraction (XRD) analysis and N_2 adsorption–desorption isotherm experiments show that the well-ordered hexagonal structure of MCM-41 is preserved and that the Mn_{12} clusters are inside the pores. The magnetic properties of the MCM-41/**1** nanocomposite material indicate that the structure of the cluster is maintained after incorporation into the MCM-41 walls, but some differences appear that may be attributed to partial substitution of carboxylate groups of **1** by silanol groups of the wall surface. In contrast with the pristine Mn_{12} derivatives calcination of the composite samples gives rise to materials with similar properties to those observed before calcination.

Keywords: Host–guest systems; MCM-41; Mesoporous materials; Single-molecule magnets; Magnetic properties; Mn clusters

1. Introduction

In 1992 Kresge et al. reported the synthesis of mesoporous silica MCM-41 that possesses ordered channels arranged in a hexagonal lattice with uniform pore sizes ranging from 20 to 100 Å in diameter [1,2]. This discovery allowed to incorporate large molecules into the cavities of these mesoporous materials. Semiconductor clusters, organic molecules and even molecular wires have been hosted by the mesoporous matrix wherein the structural confinement induced by the inorganic framework allows tailoring of the optical, electronic and magnetic properties of the nanocomposite [3].

The mixed-valence manganese clusters $[Mn_{12}O_{12}(carboxylato)_{16}]$ (carboxylato = acetate, benzoate,...), referred to as Mn_{12} are motivating a current excitement in molecular magnetism as they can act below 4 K as single-molecule nanomagnets [4,5]. Thus, at 2 K they show large magnetic hysteresis comparable to that observed in hard magnets opening the way to store information at the molecular level. On the other hand, these nanomagnets provide unique examples to observe the quantum tunneling of an electron spin through a potential barrier from one orientation to another [6–8].

In this paper, MCM-41 matrices have been used to host the Mn_{12} molecular nanomagnets in order to obtain ordered arrays of these magnetic clusters within the hexagonal channels of this mesoporous silica. The magnetic properties and thermal stability of these clusters inside the MCM-41 channels are investigated.

Recently, the acetate and benzoate derivatives of Mn_{12} have been incorporated within another mesoporous silica of the SBA-15 type [9]. This mesoporous silica is obtained by using nonionic amphiphilic triblock copolymers as organic structure-directed agent instead of the cationic alkyltrimethylammonium surfactants used for MCM-41. With this method it has been

* Corresponding author. Fax: +34-96-386-4859.
E-mail address: eugenio.coronado@uv.es (E. Coronado).

0277-5387/03/$ - see front matter
doi:10.1016/S0277-5387(03)00227-4

possible to prepare well-ordered hexagonal mesoporous silica with a tunable pore size (up to 300 Å) much larger than that presented for MCM-41 [10,11]. The incorporation of Mn_{12} clusters into the smaller pore MCM-41 mesoporous silica reported by us presents a different behavior that will be discussed.

2. Experimental

2.1. Synthesis

The four Mn_{12} derivatives used in this work were synthesized following the methods described in literature for $[Mn_{12}O_{12}(O_2CR)_{16}(H_2O)_4]$ (R = CH_3 (**1**) [12], CH_3CH_2 (**2**) [13], C_6H_5 (**3**) [14], C_6F_5 (**4**) [15]). The MCM-41 synthesis followed the method described by Kloetstra et al. with small modifications [16]. MCM-41 modified with chlorotrimethylsilane was obtained by a method described in literature [17]. The clusters were incorporated into the calcined MCM-41 by adding 100 mg of the calcined mesoporous silica to a concentrated solution of the cluster (20 mg of **1**, **2** or **4** dissolved in 10 ml of CH_3CN or 20 mg of **3** dissolved in 4 ml of CH_2Cl_2) and refluxing the mixture for 2 h. The powder was filtered and the process was repeated another time. The powder was collected by filtration and washed thoroughly with the reaction solvent.

2.2. Analysis and measurements

Gravimetric analysis was performed on a Mettler Toledo TGA/SDTA/851^e thermal analyzer. The samples were heated in flowing air at a rate of 5 °C min^{-1}. Mn analysis was performed with an atomic absorption spectrophotometer UNICAM 939 equipped with a Mn lamp. Powder XRD patterns were recorded at room temperature on a Siemens D500 diffractometer equipped with a Cu Kα source. N_2 adsorption–desorption isotherms were collected on a Micromeritics 2010 Gas adsorption Analyzer after the samples were evacuated at 373 K and 10^{-6} Torr for 10 h. Magnetic measurements were made on a Quantum Design MPMS-XL-5 susceptometer equipped with a SQUID detector from 2 to 300 K.

3. Results and discussion

3.1. Synthesis

The incorporation of Mn_{12} clusters into MCM-41 was carried out by refluxing a mixture formed by the mesoporous silica and a concentrated solution of the cluster. The reaction was carried out also at room temperature. The materials obtained by this last method present similar XRD patterns and magnetic properties but the Mn content calculated from atomic absorption spectroscopy is smaller. In order to incorporate the maximum amount of Mn_{12} we used the refluxing method. Four Mn_{12} derivatives were used, namely $[Mn_{12}O_{12}(O_2CR)_{16}(H_2O)_4]$ (R = CH_3 (**1**) [12], CH_3CH_2 (**2**) [13], C_6H_5 (**3**) [14], C_6F_5 (**4**) [15]). Acetonitrile was used as solvent for **1**, **2** and **4** and dichloromethane for **3**. The treatment of MCM-41 powders with concentrated solutions of Mn_{12} seems to be effective only for **1** and **2**. In these two cases a powder with an intense brown color was obtained while for **3** and **4** the MCM-41 powder acquired a very pale brown color. These results were confirmed by atomic absorption Mn analysis. The samples obtained after treatment with **1** and **2** showed, respectively, a Mn content of 7 and 3.5% in weight, while the Mn content for the samples treated with the two benzoate derivatives is much lower (1.2% for **3** and 0.4% for **4**). The calculated pore diameter of the calcined MCM-41 used to incorporate the Mn_{12} clusters was 25.8 Å (see below). The fact that the clusters with larger radius such as **3** or **4** cannot be incorporated within the mesoporous silica indicates that the clusters **1** and **2** are located inside the channels of the mesoporous silica and not adsorbed into the grain boundaries. Indeed, we see that the Mn content diminishes at increasing cluster radius. In order to prove this hypothesis we modified the MCM-41 surface with a silylation agent such as chlorotrimethylsilane (TMS) [17]. The effect of sylylation was to narrow the pore radius in 4.5 Å [2]. Due to the decrease in the pore diameter (25.8–16.8 Å), the channels of the MCM-41 were not sufficiently large to allow neither **1**, that is the smallest Mn_{12} derivative (maximum 17 Å), nor the other Mn_{12} derivatives to be incorporated into the modified MCM-41. This was confirmed by the experimental results that showed that none of the four Mn_{12} derivatives used in this study can be immobilized in the modified MCM-41. The incorporation of **1** and **2** in a mesoporous silica of such small pore diameter contrasts with the results obtained by Coradin et al. [9]. These authors found that **1** could not be incorporated inside a SBA-15 mesoporous silica with a similar pore diameter (25 Å).

3.2. Thermogravimetric analysis

The thermal decomposition of **1** inside the channels of MCM-41 has been studied by thermogravimetric analysis (TGA). The TGA of the MCM-41/**1** nanocomposite material in a stream of air differs significantly from that for the unmodified MCM-41. The weight loss in the temperature range from 298 to 513 K is substantially larger than that of the pure MCM-41. Whereas a weight loss of 13% is found for the MCM-41/**1** nanocomposite material, pure MCM-41 presents a weight loss of 4% working in the same conditions. Above 513 K a constant

weight is achieved. At this temperature the decomposition of the carboxylate ligands is complete as confirmed by elemental chemical analysis that indicates the lack of C. Under the same experimental conditions the thermal decomposition of **1** shows a total weight loss of 53% occurring in three steps. This weight loss corresponds to the complete removal of the acetate ligands and the water molecules. Thus, the XRD pattern of the product obtained after calcination of **1** presents the characteristic peaks of Mn_3O_4, a Mn^{II}/Mn^{III} mixed spinel. Interestingly, the XRD pattern of the calcined MCM-41/**1** does not show those peaks (see below). The MCM-41/**1** sample loses the organic ligands in the same temperature range but the process is much more gradual. Since we can deduce a 20% of **1** inside the MCM-41 from Mn analysis, we should expect a weight loss of 10.6%. This value is consistent with the experimental data from TGA.

3.3. Structural characterization

The MCM-41/**1** composite, together with the starting pure MCM-41 mesoporous silica and the MCM-41/**1** material calcined at 673 K, are characterized by XRD. The absence of diffraction peaks at $2\theta > 7^\circ$ allows to exclude segregation of Mn_{12} clusters or Mn-oxide after impregnation and calcination, respectively. Moreover, this fact suggests that good cluster dispersion along the pore walls has been achieved. Fig. 1 presents a comparison of the low angle scattering regime ($2\theta < 10^\circ$) that shows the preservation of the ordered hexagonal array of MCM-41 after Mn_{12}-functionalization as well as after calcination. Thus, all materials display XRD patterns with one strong diffraction peak in the low angle region, which usually is associated to the (1 0 0) reflection of the hexagonal cell. Apart from this intense peak, we can observe three other resolved weak reflections, that can be indexed to the (1 1 0), (2 0 0) and (2 1 0) reflections of the typical hexagonal cell. Their observation constitutes a clear probe of the existence of highly ordered hexagonal pore systems. Not only the symmetry is preserved, but also the a_0 parameter remains practically unchanged (≈ 4.14 nm). The only difference between the three patterns affects the peak intensities. Thus, the peaks in the XRD pattern of the MCM-41/**1** material are strongly reduced in intensity ($\approx 70\%$) when compared to the starting MCM-41. This loss in intensity does not imply a decrease in the long-range order or a partial collapse of the pore system. It is due to the fact that the insertion of scattering material (Mn_{12} clusters) into the pores leads to an increased phase cancellation between scattering from the walls and the pore regions. This behavior has also been observed in other systems [18] and explained by theoretical models [19].

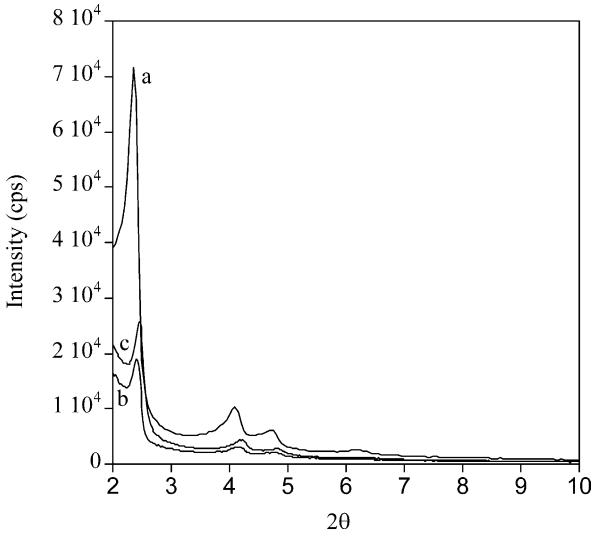

Fig. 1. XRD patterns of (a) MCM-41; (b) MCM-41/**1** and (c) MCM-41/**1** calcined at 400 °C.

Mesoporosity of all samples is further illustrated by the N_2 adsorption–desorption isotherms and the pore size distributions (Fig. 2). All samples show typical Type IV curves with one well-defined step at intermediate partial pressures ($0.2 < P/P_0 < 0.5$), which is related to the capillary condensation of N_2 inside the mesopores. The absence of hysteresis loops as well as their sharp curvature, confirm the existence of unimodal pore size distribution. In the case of the MCM-41/**1** the amount of physisorbed nitrogen decreases accompanied with a shift of the inflection point of the step to a smaller value of relative pressure. Both effects can be attributed to the inclusion of Mn_{12} clusters into the mesopores. The first effect is due to a smaller specific surface area (BET surface area decreases from 1087.7 to 729.7 $m^2\,g^{-1}$ after impregnation) and the second one is due to a significant reduction of the effective pore size (from 2.58 to ≈ 2.22 nm). Note that the incorporation of manganese itself leads to a decrease in the BET area. After impregnation, a significant broadening and asymmetry of the BJH pore size distribution occurs. These results clearly indicate coating of the pore walls and even partial filling. Finally, after calcination, the sharp isotherm

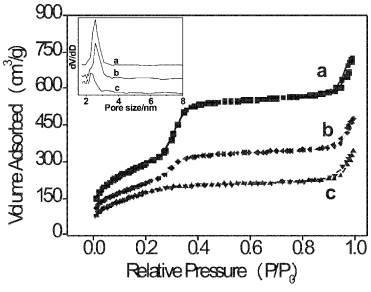

Fig. 2. N_2 adsorption–desorption isotherms (at the same scale and shifted for clarity) of (a) MCM-41; (b) MCM-41/**1** calcined at 400 °C and (c) MCM-41/**1**. The inset shows the pore size distributions.

curvature characteristic of the MCM-41 materials is recovered. The pore volume and pore size increase as consequence of the removal of the acetate ligands (see Table 1).

3.4. Magnetic properties

Fig. 3(a) shows the out-of-phase ac-susceptibility of MCM-41/**1** as a function of temperature. A clear peak is observed around 3 K which is shifted towards higher temperatures at increasing frequencies. The temperature of this peak is slightly smaller than that found for pure **1** [20]. This behavior is one of the main features of the single-molecule magnets. Analysis of the frequency dependence of the maximum of these peaks allows to calculate the anisotropy barrier and the relaxation time of the cluster ($U_{\text{eff}} = 64.7$ K and $\tau_0 = 1.39 \times 10^{-10}$ s). The values obtained are close to those of the parent crystalline compound **1**. The magnetization data vs. the applied magnetic field performed at 2 K (see Fig. 3(b)) show a hysteresis loop with coercive field of approximately 500 Oe. The coercive field at 2 K is strongly reduced by an order of magnitude when comparing to samples of **1**. This is surely related to the different spin dynamics of the Mn_{12} cluster in these two media, as it is submitted to different environments and packings. The magnetic susceptibility measurements of the MCM-41/**1** sample differ from the behavior observed on microcrystalline samples. Thus, whereas the microcrystalline samples show upon cooling down an increase in $\chi_m T$ with a maximum at 10–20 K followed by a decrease, the MCM-41/**1** sample exhibits a gradual decrease of $\chi_m T$ from 300 to 20 K and a sharp decrease below 20 K (see Fig. 4). The $\chi_m T$ value per Mn was calculated by taking into account the results of Mn analysis. These values are close at high temperatures to the values obtained for pure samples of **1**. A possible explanation for the differences observed is the possible partial substitution of acetate and water ligands of **1** by silanol groups from the walls of the MCM-41 channels.

Magnetic properties of calcined MCM-41/**1** do not show great changes with respect to the non-calcined one. The out-of-phase ac-susceptibility peaks appear at very similar temperatures but they are broader in the calcined sample (Fig. 5(a)). It presents a hysteresis loop of magnetization with a coercive field of 800 Oe that is

Table 1
Summary of the data obtained from N_2 adsorption–desorption isotherms

	S_{BET} ($m^2\,g^{-1}$)	BJH pore size (nm) [a]	Volume ($cm^3\,g^{-1}$)
MCM-41	1087.7	2.58	1.17
MCM-41/**1**	729.7	2.22	0.51
Calcined MCM-41/**1**	728.1	2.53	0.8

[a] Pore diameters calculated by using the BJH model on the adsorption branch of the isotherms.

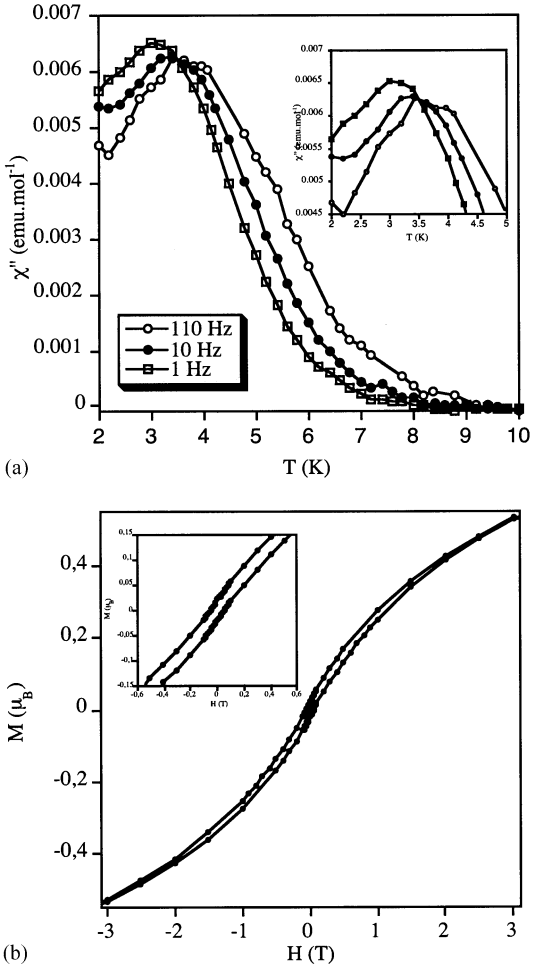

Fig. 3. T-dependence of the out-of-phase ac-susceptibility (a) and hysteresis loop of magnetization (b) of MCM-41/**1** calculated per Mn atom.

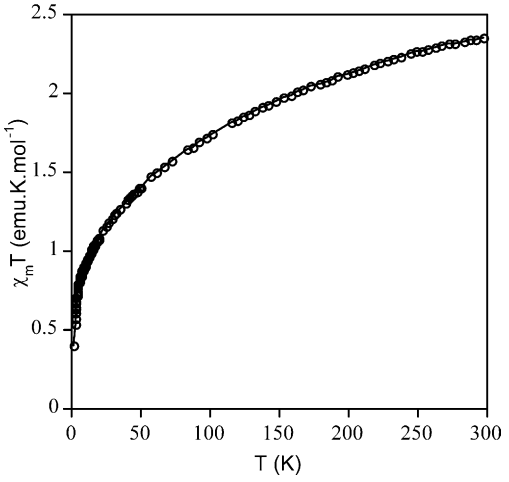

Fig. 4. T-dependence of $\chi_m T$ of MCM-41/**1** calculated per Mn atom.

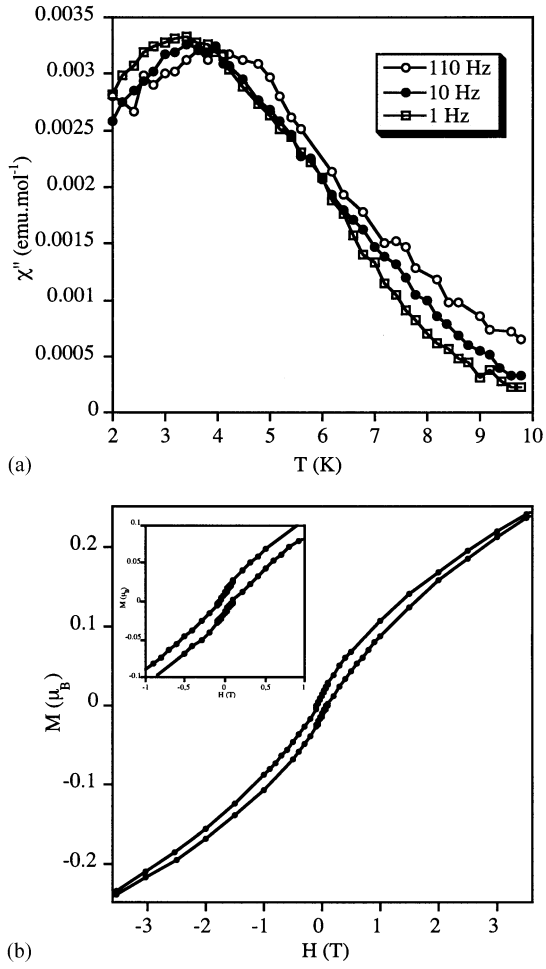

Fig. 5. T-dependence of the out-of-phase ac-susceptibility (a) and hysteresis loop of magnetization (b) of MCM-41/**1** calcined at 400 °C calculated per Mn atom.

slightly larger than that of the non-calcined samples (Fig. 5(b)). The plot of $\chi_m T$ vs. T is also similar (see Fig. 6). These data indicate that despite the removal of all the organic ligands, the core structure of the magnetic cluster is maintained. This behavior is in sharp contrast with that observed for **1** that gives rise to Mn_3O_4 after calcination. This compound is a ferrimagnet with a critical temperature of 41 K. A possible explanation is that MCM-41 stabilizes the core of the cluster by coordination with the silanol groups of the silica walls even after removal of all the organic ligands. The presence of the cluster inside the silica channels thus prevents the decomposition of the inorganic cluster.

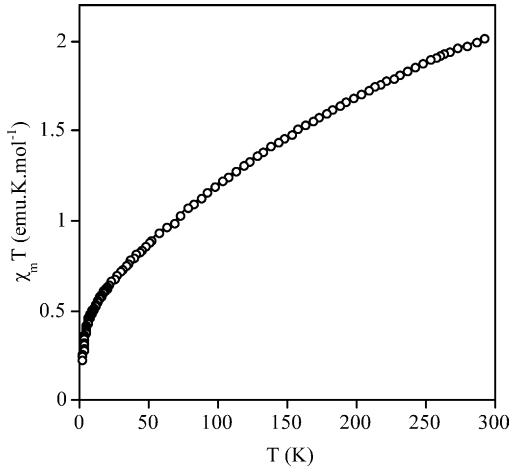

Fig. 6. T-dependence of $\chi_m T$ of MCM-41/**1** calcined at 400 °C calculated per Mn atom.

4. Conclusions

In this work we have shown that it is possible to incorporate Mn_{12} clusters within the pores of a MCM-41 mesoporous silica. Structural characterization by XRD and N_2 adsorption–desorption experiments show that the well-ordered hexagonal structure of MCM-41 is preserved and that the Mn_{12} clusters are inside the pores. The magnetic properties of the MCM-41/**1** nanocomposite material indicate that the structure of the cluster is maintained after incorporation into the MCM-41 walls but some differences appear that can be attributed to partial substitution of carboxylate groups by silanol groups from the wall surface. Calcination of the samples gave rise to a material with similar properties to those observed before calcination. Hence, we can conclude that new Mn-oxide clusters have been formed after the loss of the carboxylate ligands of Mn_{12} inside the MCM-41 pores. Further characterization of these materials by other techniques such as EPR, EXAFS and Si-NMR is in progress in order to understand the possible coordination of Si–O groups to the Mn clusters and the oxidation state of Mn.

Acknowledgements

This work was supported by the Spanish Ministerio de Ciencia y Tecnología (MCyT) (Grant MAT2001-3507-C02-01) and by the European Union (Network Molnanomag). M.C.-L. thanks the MCyT for a RyC contract. A.F.-A. thanks the Universidad de Valencia for a predoctoral fellowship.

References

[1] C.T. Kresge, M.E. Leonowicz, W.J. Roth, J.C. Vartuli, J.S. Beck, Nature 359 (1992) 710.
[2] J.S. Beck, J.C. Vartuli, W.J. Roth, M.E. Leonowicz, C.T. Kresge, K.D. Schmitt, C.T.-W. Chu, D.H. Olson, E.W. Sheppard, S.B. McCullen, J.B. Higgins, J.L. Schlenker, J. Am. Chem. Soc. 114 (1992) 10834.
[3] N.K. Raman, M.T. Anderson, C.J. Brinkler, Chem. Mater. 8 (1996) 1682.

[4] D. Gatteschi, A. Caneschi, L. Pardi, R. Sessoli, Science 265 (1994) 1054.
[5] R. Sessoli, D. Gatteschi, A. Caneschi, M.A. Novak, Nature 365 (1993) 141.
[6] J. Friedman, M.P. Sarachik, J. Tejada, R. Ziolo, Phys. Rev. Lett. 76 (1996) 3830.
[7] L. Thomas, F. Lionti, R. Ballou, D. Gatteschi, R. Sessoli, B. Barbara, Nature 383 (1996) 145.
[8] B. Schwarzschild, Phys. Today 50 (1997) 17.
[9] T. Coradin, J. Larionova, A.A. Smith, G. Rogez, R. Clérac, C. Guérin, G. Blondin, R.E.P. Winpenny, C. Sanchez, T. Mallah, Adv. Mater. 14 (2002) 896.
[10] D. Zhao, J. Feng, Q. Huo, N. Melosh, G.H. Fredickson, B.F. Chmelka, G.D. Stucky, Science 279 (1998) 548.
[11] D. Zhao, Q. Huo, J. Feng, B.F. Chmelka, G.D. Stucky, J. Am. Chem. Soc. 120 (1998) 6024.
[12] T. Lis, Acta Crystallogr. B 36 (1980) 2042.
[13] H.J. Eppley, H.-L. Tsai, N. de Vries, K. Folting, G. Christou, D.N. Hendrickson, J. Am. Chem. Soc. 117 (1995) 301.
[14] R. Sessoli, H.-L. Tsai, A.R. Shake, S. Wang, J.B. Vincent, K. Folting, D. Gatteschi, G. Christou, D. Hendrickson, J. Am. Chem. Soc. 115 (1993) 1804.
[15] T. Kuroda-Sowa, M. Lam, A.L. Rheingold, C. Frommen, W.M. Reiff, M. Nakano, J. Yoo, A.L. Maniero, L.-C. Brunel, G. Christou, D.N. Hendrickson, Inorg. Chem. 40 (2001) 6469.
[16] K.R. Kloetstra, M. van Laren, H. van Bekkum, J. Chem. Soc., Faraday Trans. 93 (1997) 1211.
[17] A.K.-W. Cheng, W.-Y. Lin, S.-G. Li, C.-M. Che, W.-Q. Pang, New J. Chem. 23 (1999) 733.
[18] F.J. Brieler, M. Fröba, L. Chen, P.J. Klar, W.F. Heimbrodt, H.-A. Krug Von Nidda, A. Loidl, Chem. Eur. J. 8 (2002) 185.
[19] W. Hammond, E. Prouzet, S.D. Mahanti, T.J. Pinnavaia, Microporous Mesoporous Mater. 27 (1999) 19.
[20] M. Evangelisti, J. Bartelomé, F. Luis, Solid State Commun. 112 (1999) 687.